ADVANCED MATERIALS TECHNOLOGIES
www.advmattechnol.de

Low-Cost, Facile, and Scalable Manufacturing of Capacitive Sensors for Soft Systems

*Edward L. White, Michelle C. Yuen, Jennifer C. Case, and Rebecca K. Kramer**

In the field of soft robotics there is a need for robust and reliable large-deformation strain sensing. Further, the field needs a way to produce such sensors in large quantities and at low cost. Toward these goals, the fabrication of highly stretchable capacitive strain sensors made from conductive elastomer composites is described here. Two novel methods of manufacturing these sensors directly onto a fabric substrate are developed: direct writing of elastomer using an extrusion process and screen printing of elastomer patterns. The effect of material processing parameters on the parameters of the finished composite films is studied and it is determined that the process is robust to a wide range of variations. The performance of sensors produced on fabric substrates is shown to be similar between the two fabrication processes. Further, the sensors are highly deformable with consistent performance up to 250% strain, and are reliable, with no changes in performance observed at 1000 cycles. It is also demonstrated that the sensors continue to perform with reduced gauge factors up to 100 000 cycles. For comparison, free-standing capacitive sensors are also produced with the same materials and it is shown that these devices are equally stable and robust. In conclusion, the fabrication process demonstrated here is robust to process variations and is capable of producing sensors directly on fabric substrates, which facilitates the production of large arrays of sensors without the need for an additional assembly step.

1. Introduction

The field of soft robotics presents the opportunity to create devices with capabilities totally unlike traditional rigid devices. From mobile robots[1] to wearable systems[2,3] to fabric-based sensory skins,[4] highly stretchable devices allow us to address challenges in new ways. Soft robots, wearable devices, and biological systems have lower elastic moduli than are found in traditional engineering materials,[5] such as metals,[6] which leads to incompatibilities and interface mismatches. Because soft systems often undergo strains on the order of 100%, commercially available strain gauges are not a compatible solution, as they typically measure strains on the order of 10%. Therefore, there is a need to develop highly deformable, electrically conductive materials with moduli similar to nontraditional soft materials such as elastomers or biological tissues.[7] In addition, soft systems often lack defined joints and exhibit continuous and distributed deformation, complicating state measurements. One solution for tracking these large continuous deformations is to distribute large numbers of strain sensors across the surface of a soft structure.

Our focus is on the development of sensory skins, which are planar substrates embedded or affixed with distributed sensors that can be wrapped and secured to the surface of a host structure.[8] In order to achieve this goal, we require scalable and robust methods to create many sensors of arbitrary geometry and configuration on a single substrate at low cost. One approach is to directly fabricate elastomer-based sensors onto a fabric substrate. Our sensors are made from a composite material which relies on expanded intercalated graphite (EIG) to achieve electrical conductivity. Conductive elastomer composites are a well-developed field[9–13] and EIG specifically has a long history.[10,14–19] We describe three approaches to making strain sensors using the same materials: (1) direct writing and (2) screen printing of finished-shape sensors directly onto a substrate and (3) a film-based process to produce free-standing sensors which can be affixed to a substrate as a subsequent step. We have chosen to focus on fabric as the substrate because of its conformability and tear-resistance. The fabric-based approaches reduce the number of manufacturing steps required to produce a sensory skin and utilize methods compatible with roll-to-roll systems for scalable, in situ manufacture of strain sensors. Through characterization of the sensors, we found that the performance and functionality of the sensors is robust to process variance, from graphite exfoliation to material deposition, and the sensors manufactured by different methods exhibit similar performance. These devices could be used to provide sensor data to soft robotic systems[20–26] or to measure human motion or pose.[2,27,28]

2. Graphite Exfoliation

The first step in fabricating our sensors is the preparation of the conductive phase. There are many methods of exfoliating

Dr. E. L. White, M. C. Yuen, J. C. Case, Prof. R. K. Kramer
School of Mechanical Engineering
Purdue University
585 Purdue Mall, West Lafayette, IN 47907-2088, USA
E-mail: rebecca.kramer@yale.edu

The ORCID identification number(s) for the author(s) of this article can be found under https://doi.org/10.1002/admt.201700072.

DOI: 10.1002/admt.201700072

© 2017 WILEY-VCH Verlag GmbH & Co. KGaA, Weinheim

graphite into few-layer graphene, including mechanical, electrochemical, and thermal schemes.[15,18,19] Previously reported work has either considered how variations in processing affect material parameters, or has demonstrated how a single set of processing parameters can be used to produce a device. Our approach is different in that it focuses on component-level parameters rather than material parameters. As such, we connect variations in processing all the way through the manufacturing sequence to the performance of finished conductive composite films, focusing on the sheet resistance of the films. Using the general consensus of the methods previously reported, the process we have used is as follows (see additional details in the Experimental Section). First, graphite flakes (**Figure 1**, 1st row) are soaked in an acid mixture, intercalating the sheets of graphene comprising the graphite with sulfuric acid. The acid-intercalated graphite is then roasted in an oven to vaporize the sulfuric acid in between the graphene sheets, causing expansion of the graphite (Figure 1, 2nd row). To further separate the multi-layer graphene sheets from one another, the expanded intercalated graphite is sonicated in a solvent (Figure 1, 3rd row). Finally, the EIG-solvent mixture is mixed with silicone elastomer at 10 wt% EIG, and then cast into conductive composite films (Figure 1, 4th and 5th rows).

2.1. Screening Study

To study the graphite exfoliation process, we identified nine critical process parameters with practical ranges based on the available literature, shown in **Table 1**, and constructed a study to measure main effects of these parameters (**Figure 2**) (see Supporting Information for treatments and measurements (Section S1)). The null hypothesis for this test was that there is no difference between different parameter levels for the sheet resistance of the composite films. The significance, p, represents the probability that the two treatments are drawn from the same population. From Table 1, all of the p-values were above a chosen Type I threshold of 0.05, indicating that the we failed to reject the null hypothesis on any parameter. However, the effect sizes, η^2, were all below a chosen effect strength threshold of 0.2, indicating that none of the parameters had a practical impact on the sheet resistance.

Based on this initial screening, we determined that sonication parameters were convolved. We accounted for this effect by combining the sonication-related parameters together into specific sonication energy (sonication energy per unit mass of graphite). The resulting relationship, plotted in Figure 2b, shows that increased specific sonication energy results in smaller particles and higher sheet resistance. We fit an exponential model to the data and obtained

$$R_{\text{sheet}} = 69.10\, e^{1.007\times10^{-5} E} \tag{1}$$

where R_{sheet} is the sheet resistance in $\Omega\square$ and E is the specific sonication energy in J g^{-1}. Specific sonication energy accounts for 74.9% of the variation in the R_{sheet} measurements (R^2 value), which is a significant part of the overall variation in sheet resistance, as expected. In order to quantify the effects of the other parameters, we computed the expected sheet resistance based on this exponential model to account for the specific sonication energy, and then computed the deviation between the observation and the model. We then determined the significance of the remaining parameters, p', based on this deviation. The results of this analysis are shown in Table 1 and Figure 2c. From this second step, we tentatively concluded that roasting temperature and acid ratio have a more significant impact on material parameters, while roasting time, acid soak time, and solvent have insignificant contributions.

2.2. Response Surface Model

Based on the tentative results of the screening study, we conducted a second detailed study using a space-filling central composite experimental design to create a response surface model based on the significant parameters: specific sonication energy, roasting temperature and acid ratio (see Supporting Information for treatments (Section S2)). The goal of the response surface model was to further confirm the significance and determine the magnitude of the effect of the significant parameters on the sheet resistance of the resulting film. However, when we limited the number of parameters in the study, we found that the sheet resistance was largely unaffected by altering the values of those parameters (Figure 2d and **Table 2**). This was not unexpected, as the effect sizes of all the parameters in both the screening study and the detailed study show that none of the parameters have a practical impact on the resulting film's sheet resistance. This finding further demonstrates the robustness of the overall graphite processing procedure; nearly any combination of values chosen within the range shown in Table 1 will yield conductive composite films with relatively similar properties.

Our conclusion from this study is that specific sonication energy is the most effective way to adjust sheet resistance. As specific sonication energy increases, the EIG particle size decreases, resulting in smaller conductive filler particles in the conductive elastomer composite. Films with larger expanded graphite particles had very low resistance at the expense of poor mechanical parameters, such as a low yield strain. Conversely, films with smaller particles had superior mechanical strength but exhibited much higher resistance. Conductive composites at either of these extremes are unsuitable for high deformation sensing. By performing this study, we identified and verified the range of significant processing parameters for producing expanded graphite with the appropriate morphology for capacitive sensors. In addition to this effect, we also experimentally verified the percolation threshold of 3 wt% for this system[29] and demonstrated that increasing particle loading above 15 wt% does not significantly improve conductivity (see Supporting Information for experimental responses (Section S3)). The bolded parameters listed in Table 1 indicate those used to make the sensors for the following section of the paper.

3. Highly Deformable Strain Sensors

In order to make use of the conductive elastomer films as a sensing element, we must consider their performance as a

© 2017 WILEY-VCH Verlag GmbH & Co. KGaA, Weinheim

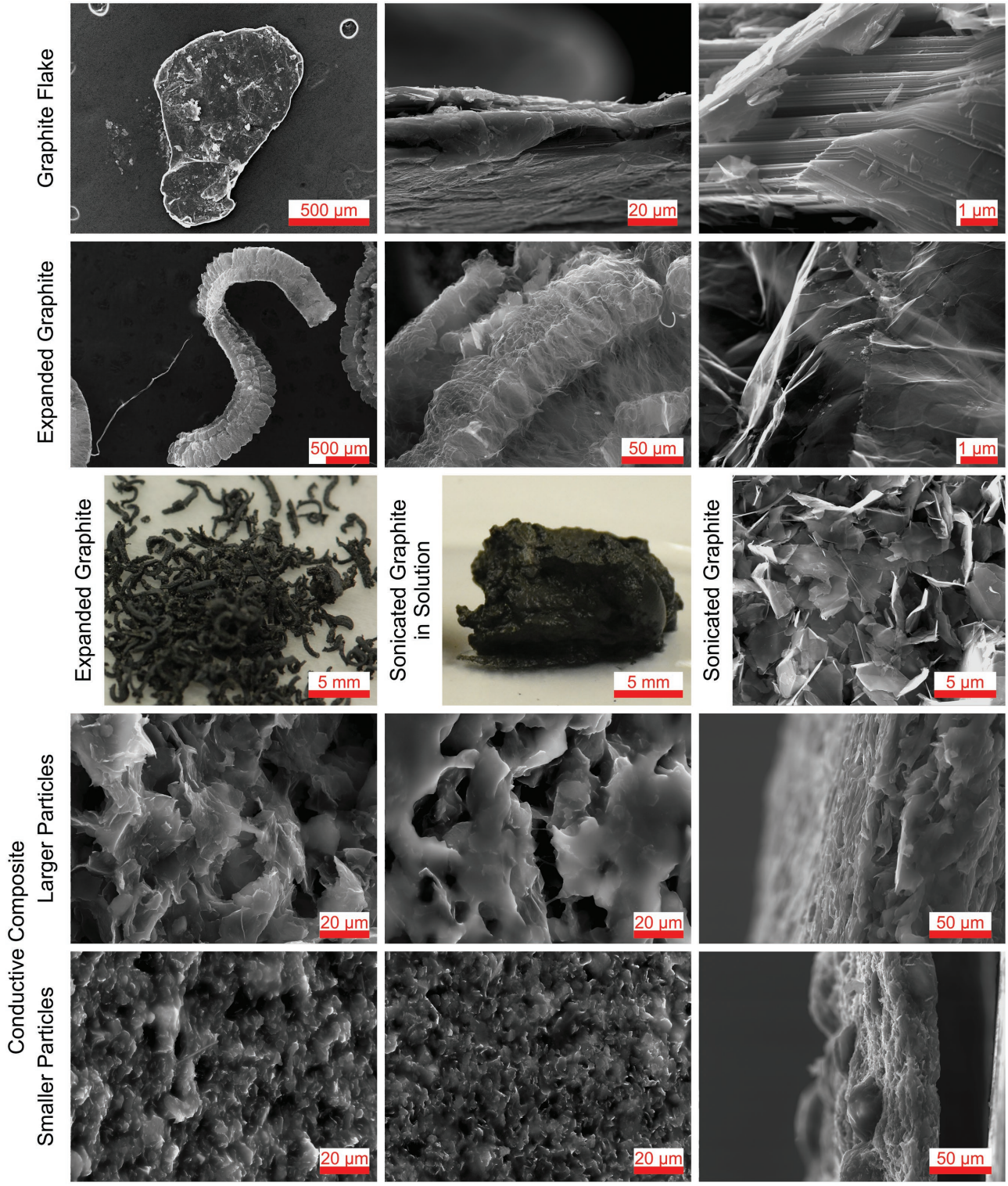

Figure 1. SEM images and photographs of the graphite exfoliation process, in order from graphite flakes (1st row), expanded graphite (2nd row), sonicated graphite (3rd row), and finally, the conductive composite (4th and 5th rows). The columns show increasing zoom from left to right.

transducer. One of the challenges of directly measuring the resistance of conductive composites in highly deformable sensors is the tendency of material properties to change over time. The change in Young's modulus and conductivity in an EIG and silicone system over many cycles was clearly illustrated by Kujawski, et al.[29] For this reason, we have elected to use

© 2017 WILEY-VCH Verlag GmbH & Co. KGaA, Weinheim

Table 1. Processing parameters evaluated in initial screening study and pro-forma study. The solvent category is not a metric scale, therefore "min" and "max" are merely labels in that case. The bolded values indicate the parameter values later used for manufacturing all sensors. The p-values (significance) and effect sizes (η^2) (measure of correlation) of the screening study and pro-forma screening study were found using ANOVA. Values associated with the pro-forma study are labeled with a′. For a parameter to be significant, we have chosen a threshold of 0.05 such that parameters with $p < 0.05$ are deemed significant. For a parameter to have sufficient effect strength, we have chosen a threshold of 0.2 such that $\eta^2 > 0.2$ are deemed significantly correlated.

Parameter	Min	Max	p	η^2	p'	η'^2
Sonication Concentration[29]	50 mL g^{-1}	**100 mL g^{-1}**	0.215	0.107	–	–
Sonication Volume	100 mL	**500 mL**	0.253	0.0899	–	–
Solvent	Toluene	**Cyclohexane**	0.302	0.0721	0.904	0.000820
Sonication Amplitude	**30**	70	0.351	0.0582	–	–
Acid Ratio[15]	3:1	**4:1**	0.374	0.0523	0.199	0.100
Sonication Time	30 min	**120 min**	0.487	0.0316	–	–
Acid Soak Time	**1 h**	24 h	0.492	0.0308	0.949	0.000231
Roast Time	**5 min**	10 min	0.505	0.0289	0.722	0.00718
Roasting Temperature[15,18]	500 °C	**800 °C**	0.764	0.00574	0.0893	0.185

capacitive sensing, which we demonstrate is more stable. Many examples of capacitive sensors appear in the soft electronics literature, including those for sensing strain, pressure, and proximity. These sensors have been made from metal electrodes,[20,30–33] carbon nanotubes,[34] liquid metals,[35–38] printed conductive inks,[39] conductive elastomers,[40,41] graphene-filled sponges,[42] conductive fibers,[43] silver nanowires,[44] and salt solutions.[45] Although these examples utilize different fabrication methods and materials, the diversity of approaches illustrates the underlying utility of capacitive sensing in many applications.

3.1. Materials and Manufacture

We fabricated our sensors from two types of elastomer: nonconductive pure silicone elastomer, which we used as a dielectric layer and support layer, and EIG-loaded elastomer, which we used as electrode layers (see Supporting Information for more details (Section S4)). For the film-based manufacturing process, we fabricated films on a sacrificial PET substrate and then folded them in half to form a three-layer structure (**Figure 3**a). In the screen-printing method, liquid

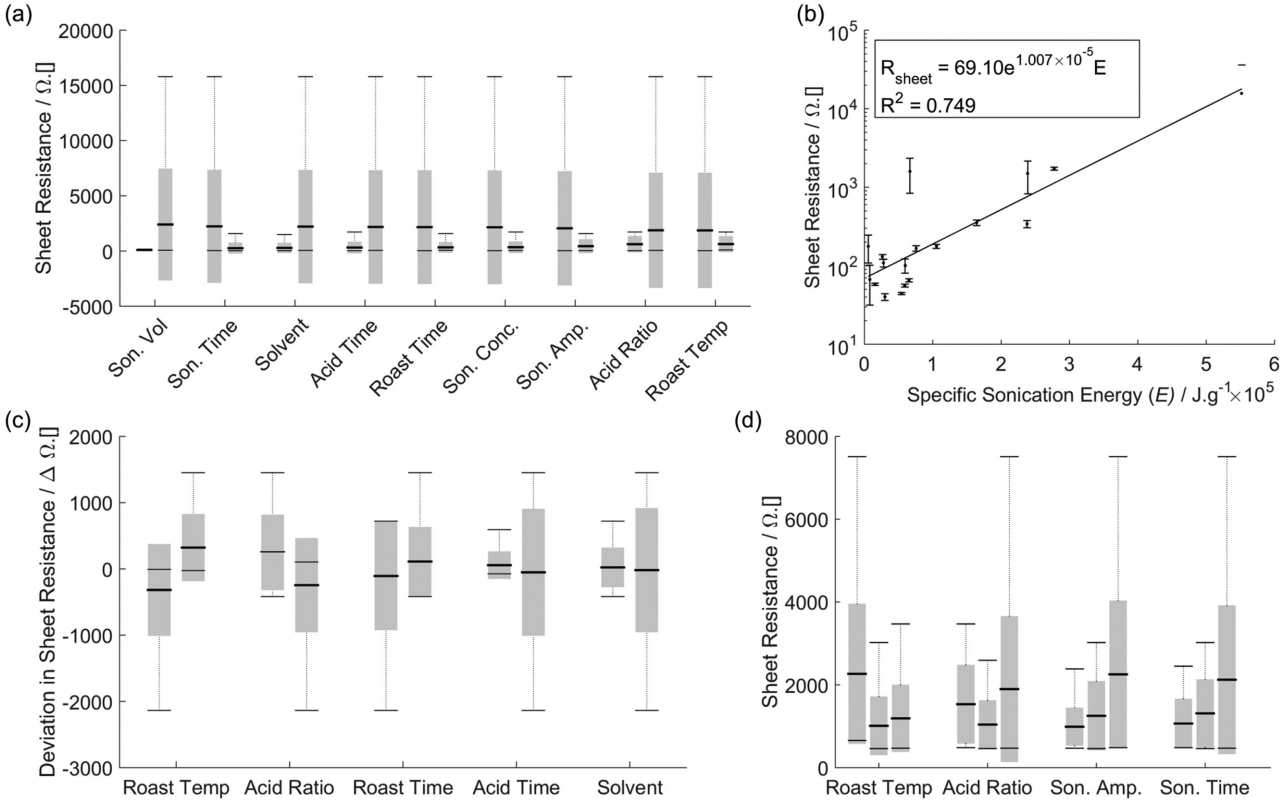

Figure 2. Results of graphite processing studies. a–c) For the box plots, the thick bar indicates the mean, the shaded rectangle is the 95% confidence about the mean, the thinner lines show the maximum and minimum sheet resistance values measured. a) Box plot comparing the sheet resistance between the min and max values of all parameters tested in the screening study. b) Sheet resistance as a function of specific sonication energy. All 18 trials of the screening study are included in this plot. 95% confidence intervals are shown based on three samples, each with three measurements. Solid line represents best exponential fit of the data. Note the logarithmic scale. c) Box plot comparing the sheet resistance between the min and max values of the pro-forma screening study. d) Box plot comparing the statistics of the response surface modeling study.

© 2017 WILEY-VCH Verlag GmbH & Co. KGaA, Weinheim

Table 2. ANOVA results of treatments evaluated in response surface model. The p-values indicate the statistical significance of the parameter, and η^2 indicates the effect size of the parameter. For a parameter to be significant, we have chosen a threshold of 0.05 such that parameters with $p < 0.05$ are deemed significant. For a parameter to have sufficient effect strength, we have chosen a threshold of 0.5 such that $\eta^2 > 0.5$ are deemed significantly correlated.

Parameter	p	η^2
Roast temperature	0.261	0.109
Acid ratio	0.708	0.0264
Sonication amplitude	0.229	0.120
Sonication time	0.319	0.0913

elastomers were rod-coated, layer-by-layer, through stencils onto Spandex fabric (Figure 3b). For the direct-writing approach, we extruded the elastomers, layer-by-layer, onto a fabric substrate using a modified commercial filament-type 3D printer (Figure 3c). The film-based manufacturing process is most similar to previously developed highly deformable sensors as it results in free-standing sensors. The screen-printing and direct-writing methods allow us to construct sensors in situ, directly patterning them onto a substrate. Once the sensor bodies are completed, each of the EIG-elastomer electrodes was electrically interfaced via copper-clad polyimide film (Figure 3d) (see Supporting Information for more details (Section S5)). Wires soldered to the copper were then run to a signal conditioning board to measure capacitance and convert it to an analog voltage output (see Supporting Information for more details (Section S6)). Following fabrication, we measured the thickness of each of the layers comprising the sensors (Figure 3e) and found that the variance in thickness across all three manufacturing methods is similar, indicating that all methods are relatively consistent. The variances of all electrode layers are very similar and the mean thicknesses are all within 40 µm of one another. The dielectric and base layers had larger variance. We believe that this is because the pure silicone elastomer has higher viscosity and will not reflow to the same extent as the EIG-loaded

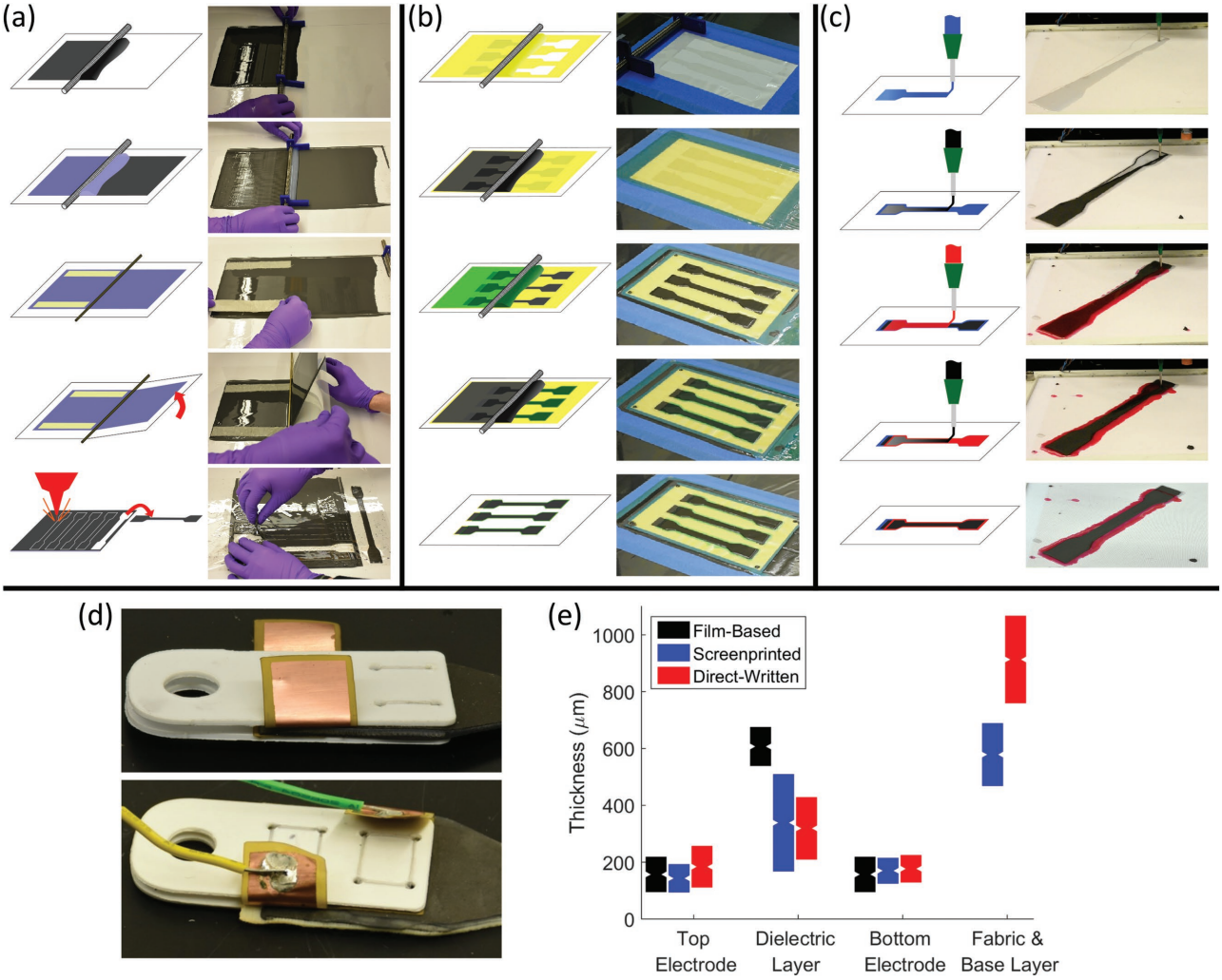

Figure 3. Sensor manufacture, assembly, and physical characterization. Schematics and photos illustrate the a) film-based, b) screen-printed, and c) direct-writing manufacturing approaches. d) Photos of the interface for the film-based and screen-printed sensors. e) Thicknesses of each layer comprising the sensors. The notch shows the mean, the bar indicates the 95% confidence bounds about the mean. The film-based sensors lack a fabric backing and thus no data are plotted.

 © 2017 WILEY-VCH Verlag GmbH & Co. KGaA, Weinheim

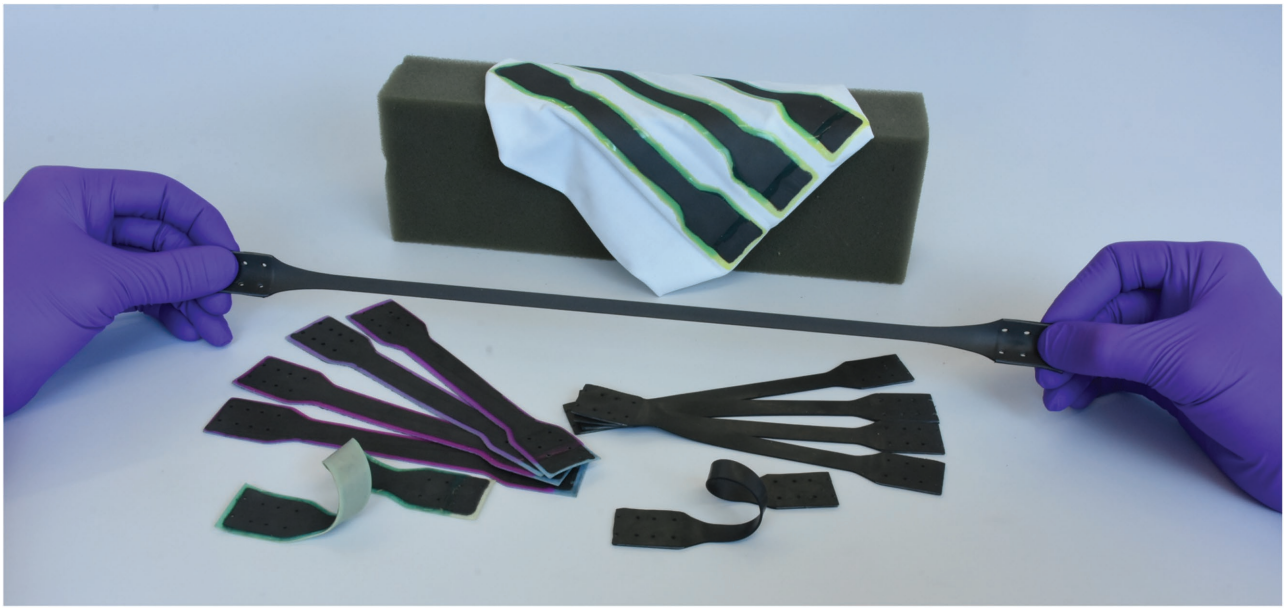

Figure 4. An assortment of sensors. At the top, a set of screen-printed sensors lay across foam block. The stretched sensor and the group of sensors on the bottom right are manufactured using the film-based method. The group of sensors on the bottom left is manufactured using direct writing.

elastomer, resulting in a less smooth film. The dielectric layer on the film-based sensors is much thicker because the film is folded over onto itself to form the devices. Despite the differences in layer thicknesses, all sensors performed similarly as shown through the following characterization tests. Sensors fabricated using all three approaches are shown in **Figure 4**.

3.2. Sensor Characterization

We first demonstrated the stability of the sensors' capacitance. We measured the resistance of the conductive composite electrodes and the unstrained sensor output (i.e., capacitance) before and after subjecting the sensors to 50 cycles of strain from 0% to 50% strain (**Figure 5**a,b). The resistance of the electrodes clearly increased as a result of the strain cycling (Figure 5a). However, the sensor output is unaffected by the 50 cycles of strain (Figure 5b). This result confirms our choice of capacitive sensing over resistive strain sensing, and additionally speaks to the robustness of the sensor functionality in operation.

We then subjected sensors to degradation testing to determine the maximum operating strain. In these tests, we cycled the sensors to a specific strain value for 10 cycles, and then incremented to the next strain value. To identify the strain at which the sensors failed, we extracted the sensor signal at its unstrained length at the end of the 10th cycle to a specific strain value, which we call dV_{10} (Figure 5c). A still-functioning sensor should show a $dV_{10} = 0$ V, i.e., the sensor returns to its initial value. We see that the dV_{10} of the fabric-based sensors begins to deviate from the ideal early on in this test. This is partially due to plastic deformation of the Spandex fabric backing, which causes the sensors to be permanently strained relative to their starting length. At strains of approximately 250%, both of the fabric-based sensors have strained to the point of failure, as indicated by the large change in the confidence bounds of the dV_{10} values. However, the film-based sensors can withstand strains to 375% until they no longer function. This test demonstrates the sensors' ability to withstand extremely large strains, such as those that may occur during installation of these sensors or during stowage and transport.

Further characterization tests showed that the sensors display similar device functionality independent of fabrication method. We first applied a low number of cycles (50) on each sensor to 50% strain to characterize the mechanical (force) and electrical (sensor signal) responses during the break-in period (Figure 5d,e). The electrical responses across all manufacturing approaches are approximately linear (Figure 5d). The linearity of the sensor response to strain simplifies the calibration process of these sensors in robotic systems. There was no noticeable transient phase in the sensor signal during the low cycle count test. The mechanical response, which displays the typical non-linear response of polymers, shows no decrease in load as the number of cycles increase (Figure 5e). The loads in the screen-printed and direct-written sensors are consistently much larger than that of the film-based sensors due to the additional fabric backing and the elastomer base layers in these sensors. We further subjected sensors to an additional 1000 cycles from 0% to 50% strain to determine behavior over repeated cycling (Figure 5f,g). The magnitude of the confidence intervals is similar between the 50 cycle and 1000 cycle tests, demonstrating that neither initial transients nor long-term degradation is present in the system. A more detailed exploration of the hysteresis and transient response of the sensors can be found in Supporting Information (Section S7). The number of cycles tested in this study is of the same order of magnitude as reported in characterization other highly deformable sensors.[46] This is an important consideration as we move from laboratory prototypes to sensors integrated into more complex devices where sensor replacement is not an option.

© 2017 WILEY-VCH Verlag GmbH & Co. KGaA, Weinheim

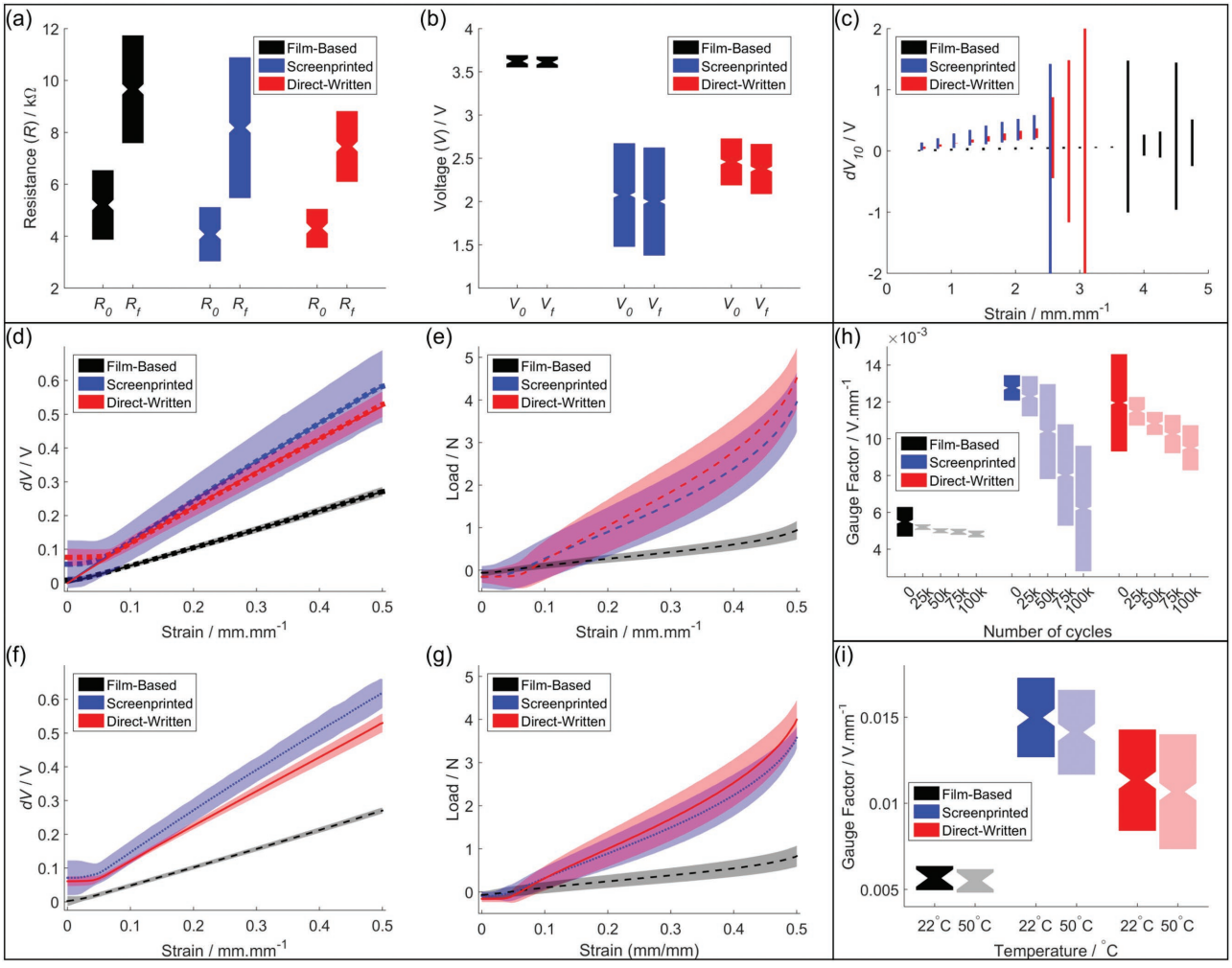

Figure 5. Sensor characterization plots. Where applicable, the data are presented as means with 95% confidence bounds. a) Comparison between the initial and final (after 50 cycles) resistances of the sensor electrodes. b) Comparison between the initial and final unstrained sensor responses. c) Plot illustrating degradation of the sensors due to strain. Three sensors from each manufacturing method were subjected to incrementally increasing strains with 10 cycles applied at each strain increment. The 95% confidence bounds of the sensor response at its unstrained length are plotted at each strain increment. Ideally, the sensors should show a dV value of 0V when unstrained; larger bars indicate degradation of sensor functionality. d–g) Plots of the electrical sensor signal (left) and mechanical (right) responses as functions of strain. dV is calculated as $V - V_0$, and is a linearly scaled measure of change in capacitance. d,e) Data from testing six sensors from each manufacturing method for the first 50 cycles. In (d), the dashed line indicates the mean response and the solid line indicates the curve fit. f,g) Data from three sensors from each manufacturing method for 1000 cycles. For details of mechanical testing, see the Experimental Section. h) Comparison of the sensor gauge factor after subjecting three sensors from each manufacturing method to 0, 25 000, 50 000, 75 000, and 100 000 cycles of strain to 50%. i) Comparison of the sensor gauge factor during testing of three sensors from each manufacturing method at ambient (22 °C) and elevated (50 °C) temperatures.

The gauge factors of the screen-printed and direct-written sensors are larger than that of the film-based sensors, as observed in the larger slopes in Figure 5d,f and as listed in **Table 3**. Because the sensors are constructed on fabric, the boundary conditions of the bottom electrode and the dielectric layer are altered. In the film-based sensors, both electrodes freely contract in the transverse direction simultaneously with the applied longitudinal stretch. In contrast, the fabric backing for the screen-printed and direct-written sensors does not contract transversely under longitudinal strain. It instead has a tendency to curl inward, maintaining its width and solely increasing in length. Under strain, the contracting transverse stress across the interface between the dielectric layer and the free top electrode is not sufficient to overcome the opposing transverse stress from the bond between the bottom electrode and the fabric/base layer. To examine this, the change in capacitance of the sensors can be modeled as

$$C = \frac{\varepsilon_0 \varepsilon_r L w}{t} = \frac{\varepsilon_0 \varepsilon_r L_0 (1+\epsilon) w_0 (1+\epsilon)^{-\nu}}{t_0 (1+\epsilon)^{\nu-1}} \tag{2}$$

$$C = C_0 (1+\varepsilon)^{2(1-\nu)} \tag{3}$$

where C is the capacitance, L and w are the length and width of the active region of the sensor, t is the thickness of the dielectric

© 2017 WILEY-VCH Verlag GmbH & Co. KGaA, Weinheim

Table 3. Gauge factors of the strain sensors during the break-in period of 50 cycles and the longer term response over 1000 cycles. The values represent the mean ± 95% confidence interval. The gauge factors correspond to the slopes of the electrical response curves shown in Figure 5d,f.

	Gauge factor	
	50 cycles	1000 cycles
Film-based	0.538 ± 0.010	0.546 ± 0.008
Screen-printed	1.13 ± 0.079	1.17 ± 0.039
Direct-written	0.983 ± 0.029	0.999 ± 0.016

layer, ε_0 is the permittivity of free space, ε_r is the relative permittivity, ε is the strain, and ν is the Poisson ratio of the sensor. The model assumes the sensor maintained constant volume and experienced inhomogeneous deformation, namely the rates of change in width ($-\nu$) and thickness ($\nu - 1$) as a function of longitudinal strain were not equal. The initial length, L_0, was 80 mm, the initial width, w_0, was 10 mm, and the average initial thicknesses of the dielectric layers, t_0, were 607, 339, and 319 µm for the film-based, screen-printed, and direct-written sensors, respectively (Figure 3e). The difference in boundary conditions is observed in a Poisson ratio, ν, of 0.350 for the film-based sensors, compared to 0.696 and 0.817 for the screen-printed and direct-written sensors, respectively. The fabric-backed sensors exhibit a planar dilation ($\nu > 0.5$) as the sensors are stretched. In addition to differences in gauge factor, at small strains, we found that the electrical responses of fabric-backed sensors (screen-printed and direct-written) are flat. This is due to plastic deformation of the relatively stiffer Spandex fabric, resulting in the sensor being slack at these small displacements after the first cycle. In implementation, these fabric-backed sensors can be precycled and prestrained to remove initial plastic effects and operate purely in the elastic region.

In addition to the 1000 cycle tests described previously, we also subjected the sensors to extended cyclic tests to determine their long-term performance. In these tests, we applied 100 000 cycles of 50% strain and measured the response after every 25 000 cycles, resulting in five total data sets per sensor. The measured gauge factors show several trends (Figure 5h). First, all three types of sensors experience decreases in gauge factor at high cycle counts. We attribute this to degradation in the conductivity of the electrode layer, which results in the electric field becoming more concentrated in the region of the interface electrodes, where the deformation is smaller than the active middle region due to the presence of the reinforcing fabric layer. Second, in the case of film-based and direct-written sensors, the confidence interval in the gauge factor decreases. We attribute this to a "break-in" effect, where variations in electrical interface conditions are removed over multiple cycles. The third result is that, although the gauge factor changes, the performance of the sensors in terms of noise and linearity is otherwise unchanged. The noise and electrical responses of all types of sensors at all cycle counts are similar to the data shown in Figure 5f, indicating that the sensors continue to function over at least a 100 000 cycle lifetime. Therefore, with appropriate recalibration processes, the sensors could continue to serve as state observers in highly deformable systems.

In order to determine the sensor response to variations in temperature, we compared sensor response at 50 °C to that at room temperature (22 °C). The resulting gauge factors are shown in Figure 5i. Although the mean gauge factors decrease for all of the sensor types, this change in mean is well within the 95% confidence intervals, indicating that it is not a statistically significant effect. Anecdotal tests at −40 °C likewise show an insignificant change in gauge factor. In summary, we conclude that effects of temperature are insignificant on the performance of the sensors, within the temperature bounds of the silicone elastomers.

The underlying theme through all of these sensor characterization tests is consistency in response. Despite large changes in the resistance of the conductive composite electrodes, the sensor signals remain stable. All of the sensors, independent of manufacturing method, display similar behavior in terms of a nearly linear electrical sensor output and a consistent mechanical response. Additionally, each sensor's performance stays self-consistent throughout operation over a large number of cycles. At larger numbers of cycles, we observe that all types of sensors experience a similar change of behavior. Of particular note, the characterization tests show that the direct-written and screen-printed sensors behave nearly identically despite differences in fabrication approach. These characterization tests indicate the suitability of these capacitive strain sensors for integration into high-deformation systems because of their insensitivity to variations in fabrication processing and their reliability during operation.

4. Conclusion

In conclusion, we have demonstrated an end-to-end process for easily realizing robust and highly deformable capacitive strain sensors using low-cost materials. We have investigated preparation of an EIG-based conductive composite material, construction of strain sensors using three fabrication methods, and response of the finished strain sensors. The conductive elastomer composite was shown to be highly robust to variations in processing conditions, with only specific sonication energy found to affect the sheet resistance and mechanical parameters of the resulting composite. We further characterized the response of sensors comprised of the EIG composite to strain over 100 000 cycles and identified their degradation behaviors. Across three distinct fabrication methods, the sensors exhibited no significant degradation in performance during cyclic testing on the order of 10^3 cycles and showed similar changes in gauge factor at the 25 000 cycle observation and beyond. Further, all sensors failed in a repeatable and consistent manner due to increasing strain during degradation testing. These studies show that expanded graphite-elastomer composites are a promising material for sensing large deformations in soft systems via capacitance. The gauge factor, ultimate strain, and cyclic performance of the sensors are comparable to other state-of-the-art soft strain sensors that are frequently used in soft robotic applications, with conductive composites demonstrating favorable robustness, ease of manufacturing, and lower cost. The three fabrication methods demonstrated herein enable simple sensor integration in a range of applications, from directly printing

© 2017 WILEY-VCH Verlag GmbH & Co. KGaA, Weinheim

strain sensors on soft robotic components to manufacturing strain-sensitive wearable garments.

5. Experimental Section

Graphite Exfoliation: The exfoliated graphite was prepared using a three step chemo-thermo-physical process. First, 5g of graphite flakes (Sigma-Aldrich) were soaked in 80 mL of sulfuric acid (Fisher Chemical) and 20 mL of nitric acid (Macron Fine Chemicals) for at least 1 h. This processed material was filtered over glass microfiber filters (934-AH, Whatman) in a Buchner filter (Z247332, Sigma-Aldrich). The filtered material was then washed with 200 mL of distilled water. After washing, the material was roasted by loading a small scoop of the material (≈3 mL) into a stainless steel cap (4981T63, McMaster-Carr) and placing it in an oven (Lindberg Blue M) set at 800 °C for 5 min. The resulting graphite exhibited a radical increase in volume over the starting material. The expanded material was further exfoliated by adding 500 mL cyclohexane (BDH1111, VWR) followed by ultrasonication at 20 kHz with an amplitude of 36 µm (30% setting) for 120 min (Q700 sonicator fitted with 1/2" tip, QSonica). After sonication, the cyclohexane and graphite mixture was more homogeneous and the large majority of the volume was a well-suspended mixture of the graphite in cyclohexane. The slurry was allowed to settle and excess solvent was decanted. Further solvent was removed by heating the slurry until a paste-like consistency was achieved, with ≈150 mL of the mixture remaining. Samples of the slurry were extracted and massed before and after drying to determine the expanded graphite concentration in each batch.

Conductive Polymer Composite: The conductive elastomer material was prepared by dispersing expanded graphite into silicone elastomer (DragonSkin 10 Slow, Smooth-On Inc.). To prepare the composite, equal parts by mass of parts A and B of the elastomer were mixed, then the required mass of expanded graphite slurry was added to achieve 10 wt% loading in the final composite. To maintain consistent material properties between batches, which had slightly different concentrations, pure cyclohexane was added to the mixture to achieve a graphite-in-slurry loading of 0.03g g^{-1}. The sheet resistance of these films was measured with a digital multimeter (5492B, BK Precision) using four-terminal resistance sensing.

Film-Based Capacitive Sensors: As a basis for comparison, stand-alone capacitive sensors were manufactured from three layers of elastomer. To do so, first a film of the conductive composite was rod-coated onto a sacrificial substrate, using the approach described in ref. [47], and this layer was allowed to cure for ≈2 h. Then a film of native silicone elastomer was rod-coated on top of the cured composite layer using the same approach to create the dielectric layer and strips of fabrics were laid onto the silicone layer to reinforce the ends of the sensors. After letting the silicone cure to a "tacky" stage, which took between 45 and 60 min, the film was folded over onto itself. After curing for ≈4 h, this stack formed the final electrode–dielectric–electrode structure. The sensors were then cut out of the film using a laser patterning system (VLS 2.30, Universal Laser Systems). Finally, water and dish soap were used to clean the soot off the sensors.

Screen-Printed Capacitive Sensors: The screen-printing process was very similar to the film-based sensor manufacturing process described above. However, instead of creating large films onto a sacrificial substrate, they were patterned directly onto a Spandex fabric substrate. Thus, these devices consisted of five layers: a fabric substrate, a base layer of insulating elastomer, a conductive bottom electrode, a dielectric layer, and a conductive top electrode. Each layer was patterned by rod-coating through a laser-cut PET mask, allowing each layer to cure in between. After all layers were patterned and cured, the sensors were cut out and cleaned with the same process as for the film-based sensors.

Direct Writing of Capacitive Sensors: Direct writing of sensors onto fabric substrates was accomplished using a modified commercial 3D printer (Simple Metal, Printrbot). The filament extruder had been removed from this device and replaced with a syringe pump. The pump was controlled using the same components as the filament drive motor. The printer was controlled with commercial software (Repetier-Host). A .stl file of the selected sensor layer was loaded into the software, and the integrated slicing algorithm (Slic3r) was used to generate a tool path in G-code. With this, the liquid elastomer could be directly extruded onto the substrate. As in the screen-printing case, one layer at a time was printed, with sufficient time between layers to achieve complete curing. After all layers were patterned and cured, the sensors were cut out using a laser patterning system.

Sensor Interface: After the sensor bodies were laser-cut and cleaned, copper interface electrodes (copper-clad polyimide film, Pyralux, DuPont) and polystyrene tabs were sewn onto the ends of the sensors. Sewing holes were laser cut through the polystyrene, copper, and sensor for alignment of layers and increased ease of assembly. Holes were laser cut through the ends of the sensor to prevent the electrode layers from shorting with each other due to sewing. Ample tension was applied during sewing to ensure that the copper electrodes had good contact against the conductive composite electrodes with polystyrene tabs.

Sensor Signal Conditioning Board: The signal conditioning boards were designed in house. A microcontroller (PIC16F1825, Microchip) was the core of this board. A charging signal was sent every 8.4 ms to charge the sensor to 2.262 V. The time it took to discharge to 0.238 V was measured. This was converted to an analog voltage signal, which was reported as the sensor response.

Mechanical and Electrical Response Testing: All sensor specimens were tested using a materials tester (Instron 4435). A 50 N load cell was used to measure the load and a voltage transducer was used to measure the analog voltage output from sensor signal conditioning board. All tests applied strain at a rate of 100% min^{-1} = 80 mm min^{-1}. The sensors were secured to the materials tester via polystyrene plates that had been sewn onto the ends of the sensor. The sensors were installed in a slack position and the crosshead of the materials tester was raised until the sensors were not slack; no further pretension was applied to the sensors.

For the cyclic fatigue testing, sensors were placed in a slider crank mechanism driven by a drill press running at 1000 rpm. After every 25 000 cycles, the sensors were removed from the slider crank mechanism and returned to the Instron to perform the same mechanical and electrical response testing as described previously. For the thermal testing, the Instron was fitted with a temperature-controlled heated environmental chamber. Samples were initially tested at room temperature in the chamber. After the initial test was completed, the chamber was activated and brought to a stable temperature at 50 °C, and the sensors were re-tested using the same method.

Supporting Information

Supporting Information is available from the Wiley Online Library or from the author.

Acknowledgements

E.L.W. and M.C.Y. contributed equally to this work. The authors would like to thank R. Adam Bilodeau for his assistance obtaining SEM images of the graphite materials and Dr. Mohammed G. Mohammed for assistance preparing the images for the manuscript. This work was supported by the National Aeronautics and Space Administration through the Early Career Faculty Program (Space Technology Research Grants Program, Grant NNX14AO52G). E.L.W. and M.C.Y. are supported by the National Science Foundation Graduate Research Fellowship (Grant DGE-1333468). J.C.C. is supported by the National Aeronautics and Space Administration's Space Technology Research Fellowship program (Grant NNX15AQ75H). The opinions and findings expressed in this paper are those of the authors, and do not necessarily reflect those of the National Aeronautics and Space Administration nor the National Science Foundation.

 © 2017 WILEY-VCH Verlag GmbH & Co. KGaA, Weinheim

Conflict of Interest

The authors declare no conflict of interest.

Keywords

additive manufacturing, conductive composite, large-deformation strain sensing, soft robotics

Received: March 20, 2017
Revised: May 17, 2017
Published online: July 24, 2017

[1] M. T. Tolley, R. F. Shepherd, B. Mosadegh, K. C. Galloway, M. Wehner, M. Karpelson, R. J. Wood, G. M. Whitesides, *Soft Rob.* **2014**, *1*, 213.
[2] Y. Menguc, Y.-L. Park, E. Martinez-Villalpando, P. Aubin, M. Zisook, L. Stirling, R. J. Wood, C. J. Walsh, in *2013 IEEE International Conference on Robotics and Automation (ICRA)*, IEEE, Karlsruhe, Germany **2013**, pp. 5309–5316.
[3] M. A. Horvath, E. T. Roche, D. M. Vogt, D. J. Mooney, F. A. Pigula, C. J. Walsh, in *ASME Proceedings on 8th Frontiers in Biomedical Devices*, ASME, Boston, MA, USA **2015**, p. V003T14A011.
[4] M. Yuen, A. Cherian, J. C. Case, J. Seipel, R. K. Kramer, in *2014 IEEE/RSJ International Conference on Intelligent Robots and Systems (IROS 2014)*, IEEE, Chicago, IL, USA **2014**, 580–586.
[5] J. A. Rogers, T. Someya, Y. Huang, *Science* **2010**, *327*, 1603.
[6] D.-H. Kim, N. Lu, R. Ma, Y.-S. Kim, R.-H. Kim, S. Wang, J. Wu, S. M. Won, H. Tao, A. Islam, K. J. Yu, T.-i. Kim, R. Chowdhury, M. Ying, L. Xu, M. Li, H.-J. Chung, H. Keum, M. McCormick, P. Liu, Y.-W. Zhang, F. G. Omenetto, Y. Huang, T. Coleman, J. A. Rogers, *Science* **2011**, *333*, 838.
[7] C. Laschi, *Proc. SPIE* **2016**, *9836*, 983626.
[8] J. Case, M. Yuen, M. Mohammed, R. Kramer, *Stretchable Bioelectronics for Medical Devices and Systems*, Springer, Switzerland, **2016**, pp. 173–191.
[9] R. F. Gibson, *Compos. Struct.* **2010**, *92*, 2793.
[10] K. K. Sadasivuni, D. Ponnamma, S. Thomas, Y. Grohens, *Prog. Polym. Sci.* **2014**, *39*, 749.
[11] M. Park, J. Park, U. Jeong, *Nano Today* **2014**, *9*, 244.
[12] S. Araby, Q. Meng, L. Zhang, I. Zaman, P. Majewski, J. Ma, *Nanotechnology* **2015**, *26*, 112001.
[13] A. Chinnappan, C. Baskar, H. Kim, S. Ramakrishna, *J. Mater. Chem. A* **2016**, *4*, 9347.
[14] D. D. L. Chung, in *Thermal Expansion 7* (Ed: D. C. Larsen), Plenum Press, New York **1982**, pp. 37–44.
[15] D. D. L. Chung, *J. Mater. Sci.* **1987**, *22*, 4190.
[16] W. Zhang, A. A. Dehghani-Sanij, R. S. Blackburn, *J. Mater. Sci.* **2007**, *42*, 3408.
[17] R. Verdejo, M. M. Bernal, L. J. Romasanta, M. A. Lopez-Manchado, *J. Mater. Chem.* **2011**, *21*, 3301.
[18] M. Cai, D. Thorpe, D. H. Adamson, H. C. Schniepp, *J. Mater. Chem.* **2012**, *22*, 24992.
[19] D. D. L. Chung, *J. Mater. Sci.* **2015**, *51*, 554.
[20] H.-K. Lee, S.-I. Chang, E. Yoon, *J. Microelectromech. Syst.* **2006**, *15*, 1681.
[21] V. Duchaine, N. Lauzier, M. Baril, M.-A. Lacasse, C. Gosselin, in *IEEE International Conference on Robotics and Automation, 2009. ICRA '09*, IEEE, Kobe, Japan **2009**, pp. 3676–3681.
[22] Y.-L. Park, B.-r. Chen, R. J. Wood, in *2011 IEEE Sensors*, IEEE, Limerick, Ireland **2011**, pp. 81–84.
[23] R. K. Kramer, C. Majidi, R. J. Wood, in *2011 IEEE International Conference on Robotics and Automation (ICRA)*, IEEE, Shanghai, China **2011**, pp. 1103–1107.
[24] Y.-L. Park, B.-R. Chen, R. J. Wood, *IEEE Sens. J.* **2012**, *12*, 2711.
[25] J.-B. Chossat, Y. Tao, V. Duchaine, Y.-L. Park, in *2015 IEEE International Conference on Robotics and Automation (ICRA)*, IEEE, Seattle, WA, USA **2015**, pp. 2568–2573.
[26] Y. Chen, M. Yu, H. A. Bruck, E. Smela, *Smart Mater. Struct.* **2016**, *25*, 055006.
[27] D. Z. Stupar, J. S. Bajic, L. M. Manojlovic, M. P. Slankamenac, A. V. Joza, M. B. Zivanov, *IEEE Sens. J.* **2012**, *12*, 3424.
[28] R. K. Kramer, C. Majidi, R. Sahai, R. J. Wood, in *2011 IEEE/RSJ International Conference on Intelligent Robots and Systems (IROS)*, IEEE, San Francisco, CA, USA **2011**, pp. 1919–1926.
[29] M. Kujawski, J. D. Pearse, E. Smela, *Carbon* **2010**, *48*, 2409.
[30] E.-S. Hwang, J.-h. Seo, Y.-J. Kim, *J. Microelectromech. Syst.* **2007**, *16*, 556.
[31] D. P. J. Cotton, I. M. Graz, S. P. Lacour, *IEEE Sens. J.* **2009**, *9*, 2008.
[32] H.-K. Lee, S.-I. Chang, E. Yoon, *IEEE Sens. J.* **2009**, *9*, 1748.
[33] J. A. Dobrzynska, M. A. M. Gijs, *Sens. Actuators, A* **2012**, *173*, 127.
[34] L. Cai, L. Song, P. Luan, Q. Zhang, N. Zhang, Q. Gao, D. Zhao, X. Zhang, M. Tu, F. Yang, W. Zhou, Q. Fan, J. Luo, W. Zhou, P. M. Ajayan, S. Xie, *Sci. Rep.* **2013**, *3*, 1.
[35] J. Wissman, T. Lu, C. Majidi, in *2013 IEEE SENSORS*, IEEE, Baltimore, MD, USA **2013**, pp. 1–4.
[36] S. Baek, D.-J. Won, J. G. Kim, J. Kim, *J. Micromech. Microeng.* **2015**, *25*, 095015.
[37] L. Sheng, S. Teo, J. Liu, *J. Med. Biol. Eng.* **2016**, *36*, 265.
[38] B. Li, Y. Gao, A. Fontecchio, Y. Visell, *Smart Mater. Struct.* **2016**, *25*, 075009.
[39] Y. Kawahara, S. Hodges, B. S. Cook, C. Zhang, G. D. Abowd, in *Proceedings of the 2013 ACM International Joint Conference on Pervasive and Ubiquitous Computing*, UbiComp '13, ACM, New York, NY, USA **2013**, pp. 363–372.
[40] G. Cannata, M. Maggiali, G. Metta, G. Sandini, in *IEEE International Conference on Multisensor Fusion and Integration for Intelligent Systems, 2008. MFI 2008*, IEEE, Seoul, South Korea **2008**, pp. 434–438.
[41] M. D. Bartlett, E. J. Markvicka, C. Majidi, *Adv. Funct. Mater.* **2016**, *26*, 8496.
[42] S. Chun, A. Hong, Y. Choi, C. Ha, W. Park, *Nanoscale* **2016**.
[43] J. Lee, H. Kwon, J. Seo, S. Shin, J. H. Koo, C. Pang, S. Son, J. H. Kim, Y. H. Jang, D. E. Kim, T. Lee, *Adv. Mater.* **2015**, *27*, 2433.
[44] S. Yao, Y. Zhu, *Nanoscale* **2014**, *6*, 2345.
[45] Y. Liang, B. Wan, G. Li, Y. Xie, T. Li, *Proc. SPIE* **2016**, *9798*, 979830.
[46] S. Kim, J. Lee, B. Choi, *IEEE Sens. J.* **2015**, *15*, 6077.
[47] E. White, J. Case, R. Kramer, *IEEE Sens. J.* **2015**, *16*, 2607.

© 2017 WILEY-VCH Verlag GmbH & Co. KGaA, Weinheim